Supplementary Information for Highly Stable Two-Dimensional Carbon Allotropes Based on Azulenoid Kekulene

Zhenzhe Zhang[a], Hanh D. M. Pham[a], Dmytro F. Perepichka[a,*], Rustam Z. Khaliullin[a,*]

[a]*Department of Chemistry, McGill University, 801 Sherbrooke St West, Montreal, H3A 0B8, Quebec, Canada*

S1. 2D carbon allotropes based on azulene

Figure S1 shows the structures and energies of the previously reported 2D carbon allotropes containing azulene units: SW-graphene [1], azugraphene [2], ψ-graphene [3], phagraphene [4], pentaheptite [5], Pza-C_{10} [6], oblique heackelite, and C-57.

S2. Stability of azulenoid kekulene

The cyclization strain energy of the azulenoid kekulene (AK) molecule was calculated by comparing its energy to that of its linear isomer (Fig. S2). Calculations were performed using Perdew-Burke-Ernzerhof (PBE) exchange-correlation functional as described in Computational methods. They indicate that the AK macrocycle is 0.16 eV/azulene unit more stable than its linearized isomer. This indicates that the strain energy of cyclization is fully compensated by the aromatic stabilization of the AK macrocycle. Thus, the low strain and aromaticity of AK explain the stability of the AK-based 2D polymers discussed in this work.

S3. Computational methods

Computational modeling was performed using density functional theory as implemented in Vienna Ab initio Simulation Package (VASP) [7, 8, 9, 10]. The projector augmented wave formalism was used to describe interactions of atomic cores with valence electrons. Electronic states were modeled using a plane wave basis set with the energy cutoff set at 520 eV. The dispersion-corrected (D3BJ) [11, 12] Perdew-Burke-Ernzerhof (PBE) generalized gradient approximation [13] was used as the exchange-correlation functional for the optimization of lattice vectors and atomic positions.

*Corresponding author

Email addresses: dmytro.perepichka@mcgill.ca (Dmytro F. Perepichka), rustam.khaliullin@mcgill.ca (Rustam Z. Khaliullin)

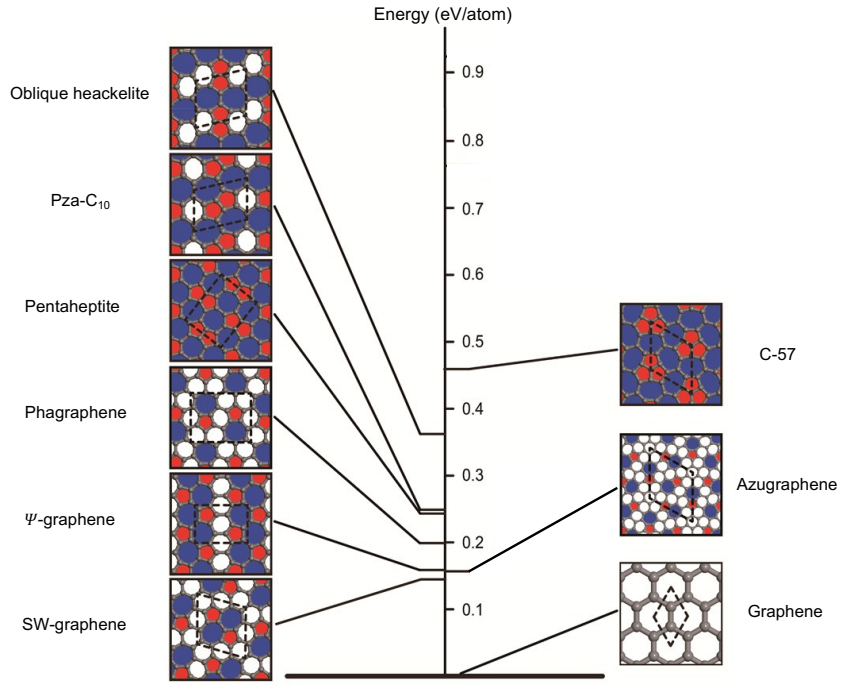

Supplementary Figure S1: Previously reported 2D carbon allotropes containing azulene units. The energy per atom above graphene is shown. The dashed lines show unit cells. Adapted from Ref. [2] with permission from the Royal Society of Chemistry.

The unit cell of 2D materials was optimized in the two lateral directions with the pressure set to zero. The cell size perpendicular to the plane was fixed at 10 Å, which is sufficiently large to make the effect of interlayer interactions on the computed properties negligibly small. For the geometry relaxation, the integration over the Brillouin zone was performed using the $11 \times 11 \times 1$ Monkhorst-Pack k-point mesh. Convergence criterion for the self-consistent field procedure was set to 1×10^{-6} eV. Atomic positions were optimized until the maximum force on atoms decreased below $0.02\,\mathrm{eV\,\AA^{-1}}$. It is important to note that setting pressure to zero ensures that the enthalpy of a 2D material $H = E + pV$ is equal to its energy. The zero pressure approximation is appropriate to describe materials at the pressure of 1 atmosphere.

Band structure calculations were carried out for the optimized structures with either the dispersion-corrected PBE or dispersion-corrected Heyd-Scuseria-Ernzerhof (HSE) exchange-correlation functionals [14, 15]. $64 \times 64 \times 1$ and $3 \times 3 \times 1$ Monkhorst-Pack k-point meshes were employed in PBE and HSE calculations, respectively. The band structures of all 2D materials were simulated and plotted along the lines connecting high symmetry points in the Brillouin zone: Γ (0,0, 0.0, 0.0) → K (2/3, 1/3, 0.0) → M (1/2, 0.0, 0.0) → Γ (0,0, 0.0, 0.0).

The effective mass of electrons and holes were calculated from the DFT band structure as curvatures of

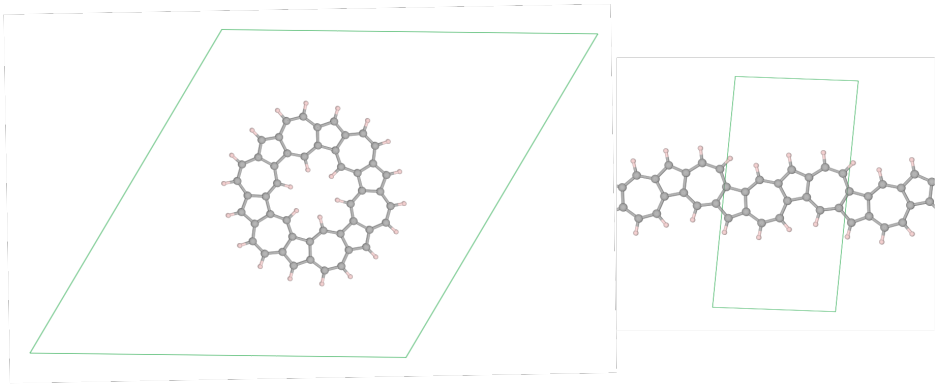

Supplementary Figure S2: Structures of the azulenoid kekulene macrocycle (left) and its linearized isomer (right).

electronic bands using the `sumo` program [16]. Effective mass for electrons (holes) is reported only for the lowest (highest) energy minimum (maximum) on conduction (valence) bands.

The PBE convex hull for hydrocarbons is defined by the hydrogen molecular crystals in the cubic α N_2 structure, solid methane in the silicon tetrafluoride polymorph, and hexagonal (ABAB) graphite.

S4. Alternative measure of stability of 2D carbon allotropes

In the main text, the stability of carbon allotropes is measured by comparing their total energy per atom to that of graphene. Although this measure is employed in all previous studies of carbon allotropes, it is important to consider its limitations for this study. If the separation between the AK units increased significantly, this measure of stability would decrease to zero, making it difficult to compare the stability of AK-based and non-AK carbon allotropes meaningfully. To make an illustrative example, AKC-$[100, 0]$ with well-separated AK units could be claimed, based on this measure, as the most stable carbon allotrope, which is meaningless because this material mostly consists of graphene.

This measure is also problematic because it makes it difficult to compare the stability among different AKCs. For example, it is unclear whether AKC-$[6, 0]$ is more stable than AKC-$[5, 1]$ because of the stronger interactions between the AK units or simply because of the larger distance between them.

In order to reduce the trivial stabilization effect due to the spatial separation between the AK units, we introduced an alternative measure of stability of azulene-based materials, AKCs and previously studied carbons. In this measure denoted E_x, the energy of the unit cell (E_{uc}) of an allotrope above the graphene is divided by the total number of non-benzoid atoms in the unit cell ($N_{nbz,uc}$), not by the total number of atoms (N_{uc}):

$$E_x = \frac{E_{uc} - N_{uc} \times E_{graphene/atom}}{N_{nbz,uc}} = \frac{N_{uc}}{N_{nbz,uc}} \left(E_{allotrope/atom} - E_{graphene/atom}\right) \tag{1}$$

Non-benzoid atoms are those that are surrounded by hexagonal rings on all sides.

Material	Energy above graphene (eV/atom)	N_{uc}	N_{nbz}	E_x (eV/atom)
AKC-[4,2]	0.108	56	48	0.126
AKC-[5,1]	0.111	62	48	0.143
AKC-[6,0]	0.102	72	48	0.153
AKC-[4,1]	0.132	42	36	0.154
AKC-[3,3]	0.156	54	48	0.175
AKC-[5,0]	0.159	50	42	0.189
AKC-[3,2]	0.189	38	32	0.224
SW-graphene	0.141	16	16	0.141
ψ-graphene	0.158	10	10	0.158
Phagraphene	0.199	20	20	0.199
Azugraphene	0.157	38	30	0.199
Pentaheptite	0.243	16	16	0.243
Pza-C_{10}	0.249	10	10	0.249
Oblique heackelite	0.362	12	12	0.362
C-57 carbon	0.459	12	12	0.459

Supplementary Table S1: Stability of carbon allotropes according to the alternative measure E_x that accounts for the presence of carbon atoms in hexagonal environments.

Table S1 shows that, according to the new measure, AKC materials described in this work are still among the most stable 2D carbon allotropes.

Another important observation enabled by E_x scale is that AKC-$[4, 2]$ stands out among the AKC structures as the material with the strongest interaction between its AK units. In this material, the pentagonal rings are directly bonded to the hexagonal rings of the neighboring AK units, making the material remarkably stable.

S5. Tentative synthetic route to PAK-$[3, 3]$

A possible synthetic route to the multigap PAK-$[3, 3]$ semiconductor with light holes and electrons can follow the procedure established for graphene nanoribbons [17]. It can use on-surface Ullmann coupling [18] of halogenated AK monomers, followed by the dehydrogenation reaction [19], as shown in Fig. S3.

S6. Parity of nodes of AK-based structures

As stated in the main text, the electronic structure of the proposed materials is to a large extent determined by the relative position of azulenoid kekulene (AK) units in the lattice. All $[6, 0]$, $[3, 3]$ and $[4, 1]$ materials are semiconductors, while the others – $[4, 2]$, $[5, 1]$, $[5, 0]$ and $[3, 2]$ – are metals or semimetals.

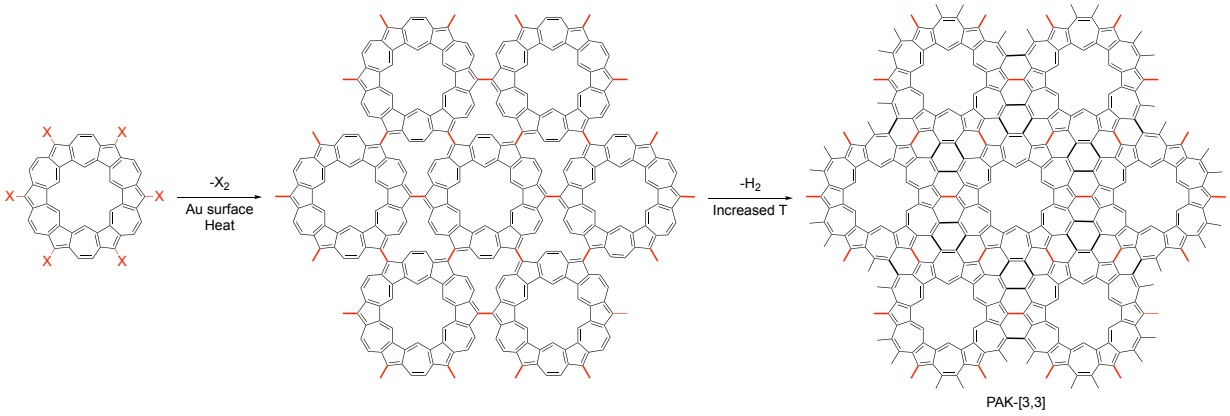

Supplementary Figure S3: Tentative synthetic route to PAK-[3, 3] based on the Ullmann coupling of the halogenated AK monomers followed by the dehydrogenation reaction. X denotes halogen atoms.

We observe that semiconductors are obtained when the nodes of the underlying porous graphene matrix are *even*, whereas semimetals or metals are obtained when the nodes are *odd*. A node of the porous graphene matrix is defined as a group of atoms forming connections to the three identical neighbor nodes. The nodes are shown with white color in Fig. 3 of the main text. A node is called *even* if there is a hexagon of carbon atoms in its center. Examples of even nodes include nodes of $[6, 0]$, $[3, 3]$ and $[4, 1]$ materials. A node is called *odd* if there is a single carbon atom in its center. Materials $[4, 2]$, $[5, 1]$, $[5, 0]$ and $[3, 2]$ contain odd nodes. Interestingly, even nodes represent closed-shell molecules with paired electrons (e.g. benzene, triphenylene, coronene), whereas odd nodes represent open-shell radicals (e.g. triangulenes).

S7. Electronic structure of molecular building blocks

Computational modeling of molecular structures was performed using density functional theory as implemented in Gaussian 16, Revision A.03 [20]. The optimization of molecular geometries and calculation of molecular orbital diagrams were carried out using PBE0 hybrid exchange-correlation functional [21, 13] in combination with the 6-31G(d) basis set. Molecular orbital diagrams for naphthalene, azulene, kekulene and azulenoid kekulene molecules are shown in Fig. S4.

The depicted molecular orbital energies elucidate that the HOMO-LUMO gap for azulene is 1.54 eV narrower than that of naphthalene. Similarly, the unoccupied molecular orbitals of azulenoid kekulene also lie lower than those of kekulene.

S8. Band structures diagrams

Band structure diagrams were calculated using the HSE exchange-correlation functional for all materials as described in Computational methods and are shown in Fig. S5.

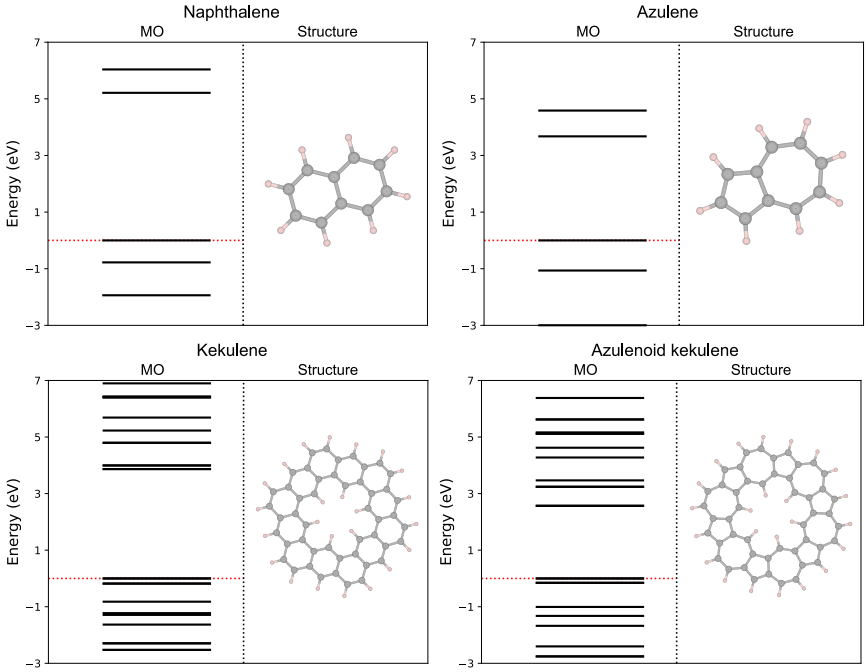

Supplementary Figure S4: PBE0/6-31G(d) molecular orbital diagrams for naphthalene, azulene, kekulene and azulenoid kekulene molecules. HOMO energies are used as the zero-energy references (dashed line).

References

[1] H. Yin, X. Shi, C. He, M. Martinez-Canales, J. Li, C. J. Pickard, C. Tang, T. Ouyang, C. Zhang, J. Zhong, Stone-Wales graphene: a two-dimensional carbon semimetal with magic stability, Phys. Rev. B 99 (4) (2019) 041405.

[2] J. Liu, H. Lu, Azugraphene: a new graphene-like hexagonal carbon allotrope with dirac cones, RSC Adv. 9 (59) (2019) 34481–34485.

[3] X. Li, Q. Wang, P. Jena, ψ-graphene: a new metallic allotrope of planar carbon with potential applications as anode materials for lithium-ion batteries, J. Phys. Chem. Lett. 8 (14) (2017) 3234–3241.

[4] Z. Wang, X.-F. Zhou, X. Zhang, Q. Zhu, H. Dong, M. Zhao, A. R. Oganov, Phagraphene: a low-energy graphene allotrope composed of 5–6–7 carbon rings with distorted dirac cones, Nano Lett. 15 (9) (2015) 6182–6186.

[5] M. P. Molepo, R. E. Mapasha, K. O. Obodo, N. Chetty, First principles calculations of pentaheptite graphene and boronitrene derivatives, Comput. Mater. Sci. 92 (2014) 395–400.

[6] X. Luo, L.-M. Liu, Z. Hu, W.-H. Wang, W.-X. Song, F. Li, S.-J. Zhao, H. Liu, H.-T. Wang, Y. Tian, Two-dimensional superlattice: modulation of band gaps in graphene-based monolayer carbon superlattices, J. Phys. Chem. Lett. 3 (22) (2012) 3373–3378.

[7] G. Kresse, J. Hafner, Ab initio molecular dynamics for liquid metals, Phys. Rev. B 47 (1) (1993) 558.

[8] G. Kresse, J. Hafner, Ab initio molecular-dynamics simulation of the liquid-metal–amorphous-semiconductor transition in germanium, Phys. Rev. B 49 (20) (1994) 14251.

[9] G. Kresse, J. Furthmüller, Efficiency of ab-initio total energy calculations for metals and semiconductors using a plane-wave basis set, Comput. Mater. Sci. 6 (1) (1996) 15–50.

[10] G. Kresse, J. Furthmüller, Efficient iterative schemes for ab initio total-energy calculations using a plane-wave basis set, Phys. Rev. B 54 (16) (1996) 11169.

[11] S. Grimme, J. Antony, S. Ehrlich, H. Krieg, A consistent and accurate ab initio parametrization of density functional dispersion correction (DFT-D) for the 94 elements H-Pu, J. Chem. Phys. 132 (15) (2010).

[12] S. Grimme, S. Ehrlich, L. Goerigk, Effect of the damping function in dispersion corrected density functional theory, J. Comput. Chem. 32 (7) (2011) 1456–1465.

[13] J. P. Perdew, K. Burke, M. Ernzerhof, Generalized gradient approximation made simple, Phys. Rev. Lett. 77 (18) (1996) 3865.

[14] J. Heyd, G. E. Scuseria, M. Ernzerhof, Hybrid functionals based on a screened coulomb potential, J. Chem. Phys. 118 (18) (2003) 8207–8215.

[15] A. V. Krukau, O. A. Vydrov, A. F. Izmaylov, G. E. Scuseria, Influence of the exchange screening parameter on the performance of screened hybrid functionals, J. Chem. Phys. 125 (22) (2006) 224106.

[16] A. M. Ganose, A. J. Jackson, D. O. Scanlon, sumo: command-line tools for plotting and analysis of periodic ab initio calculations, J. Open Source Softw. 3 (28) (2018) 717.

[17] P. Ruffieux, S. Wang, B. Yang, C. Sánchez-Sánchez, J. Liu, T. Dienel, L. Talirz, P. Shinde, C. A. Pignedoli, D. Passerone, et al., On-surface synthesis of graphene nanoribbons with zigzag edge topology, Nature 531 (7595) (2016) 489–492.

[18] Q. Fan, J. M. Gottfried, J. Zhu, Surface-catalyzed C–C covalent coupling strategies toward the synthesis of low-dimensional carbon-based nanostructures, Acc. Chem. Res. 48 (8) (2015) 2484–2494.

[19] J. Cai, P. Ruffieux, R. Jaafar, M. Bieri, T. Braun, S. Blankenburg, M. Muoth, A. P. Seitsonen, M. Saleh, X. Feng, et al., Atomically precise bottom-up fabrication of graphene nanoribbons, Nature 466 (7305) (2010) 470–473.

[20] M. J. Frisch, G. W. Trucks, H. B. Schlegel, G. E. Scuseria, M. A. Robb, J. R. Cheeseman, G. Scalmani, V. Barone, G. A. Petersson, H. Nakatsuji, X. Li, M. Caricato, A. V. Marenich, J. Bloino, B. G. Janesko, R. Gomperts, B. Mennucci, H. P. Hratchian, J. V. Ortiz, A. F. Izmaylov, J. L. Sonnenberg, D. Williams-Young, F. Ding, F. Lipparini, F. Egidi, J. Goings, B. Peng, A. Petrone, T. Henderson, D. Ranasinghe, V. G. Zakrzewski, J. Gao, N. Rega, G. Zheng, W. Liang, M. Hada, M. Ehara, K. Toyota, R. Fukuda, J. Hasegawa, M. Ishida, T. Nakajima, Y. Honda, O. Kitao, H. Nakai, T. Vreven, K. Throssell, J. A. Montgomery, Jr., J. E. Peralta, F. Ogliaro, M. J. Bearpark, J. J. Heyd, E. N. Brothers, K. N. Kudin, V. N. Staroverov, T. A. Keith, R. Kobayashi, J. Normand, K. Raghavachari, A. P. Rendell, J. C. Burant, S. S. Iyengar, J. Tomasi, M. Cossi, J. M. Millam, M. Klene, C. Adamo, R. Cammi, J. W. Ochterski, R. L. Martin, K. Morokuma, O. Farkas, J. B. Foresman, D. J. Fox, Gaussian˜16 Revision A.03, gaussian Inc. Wallingford CT (2016).

[21] C. Adamo, V. Barone, Toward reliable density functional methods without adjustable parameters: the PBE0 model, J. Chem. Phys. 110 (13) (1999) 6158–6170.

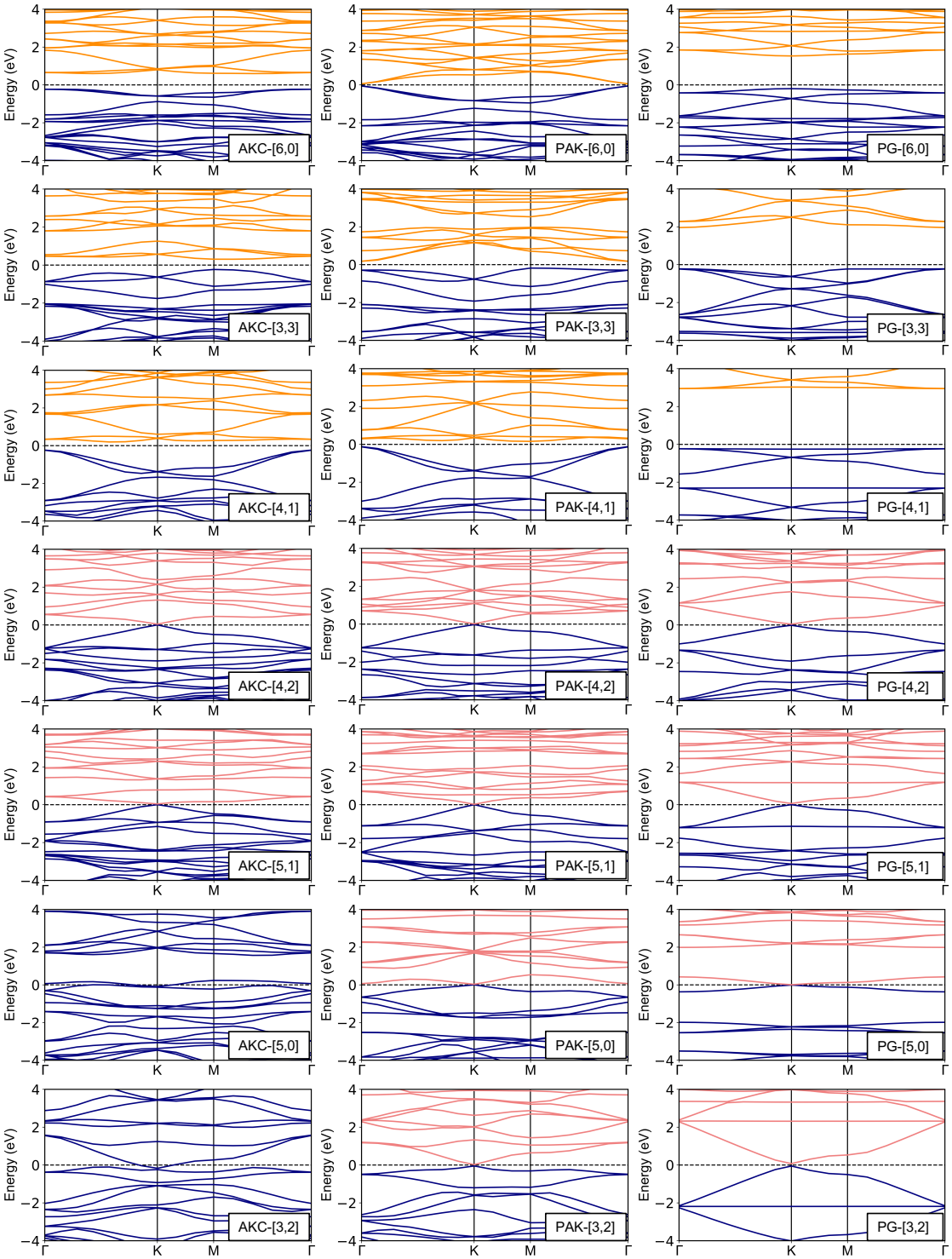

Supplementary Figure S5: HSE band structure diagrams for seven materials from the AKC (left), PAK (center) and PG (right) families. The orange color denotes conduction bands of semiconductors, the red color denotes the conduction bands of Dirac-cone semimetals, and the blue color denotes the conduction bands of metals and valence bands of all materials.